Structure of quantum disordered wave functions: weak localization, far tails, and mesoscopic transport

B.K. Nikolić[1,a] and V.Z. Cerovski[2]

[1] Department of Physics, Georgetown University, Washington, DC 20057-0995, USA
[2] Department of Physics, Virginia Commonwealth University, Richmond, VA 23284, USA

Abstract. We report on the comprehensive numerical study of the fluctuation and correlation properties of wave functions in three-dimensional mesoscopic diffusive conductors. Several large sets of nanoscale samples with finite metallic conductance, modeled by an Anderson model with different strengths of diagonal box disorder, have been generated in order to investigate both small and large deviations (as well as the connection between them) of the distribution function of eigenstate amplitudes from the universal prediction of random matrix theory. We find that small, weak localization-type, deviations contain both diffusive contributions (determined by the bulk and boundary conditions dependent terms) and ballistic ones which are generated by electron dynamics below the length scale set by the mean free path ℓ. By relating the extracted parameters of the functional form of nonperturbative deviations ("far tails") to the exactly calculated transport properties of mesoscopic conductors, we compare our findings based on the full solution of the Schrödinger equation to different approximative analytical treatments. We find that statistics in the far tail can be explained by the exp-log-cube asymptotics (convincingly refuting the log-normal alternative), but with parameters whose dependence on ℓ is linear and, therefore, expected to be dominated by ballistic effects. It is demonstrated that both small deviations and far tails depend explicitly on the sample size—the remaining puzzle then is the evolution of the far tail parameters with the size of the conductor since short-scale physics is supposedly insensitive to the sample boundaries.

PACS. 73.21.-b Electron states and collective excitations in multilayers, quantum wells, mesoscopic, and nanoscale systems – 73.20.Fz Weak or Anderson localization – 73.23.-b Electronic transport in mesoscopic systems – 05.45.Mt Quantum chaos; semiclassical methods

1 Introduction

Quantum coherence, its nonlocal features, and randomness of microscopic details can cause large fluctuations of physical quantities in disordered mesoscopic systems. The paradigmatic case is that of conductance fluctuations which has given impetus for the whole field of mesoscopic physics [1,2] by pointing out at unexpected features of such fluctuations [3]. Contrary to the intuition developed from thermal fluctuations, and their self-averaging properties in the statistical physics of macroscopic systems, the average value and variance are not enough to characterize the broad distribution functions of various mesoscopic quantities [4], even well into the metallic regime $g \gg 1$ ($g = G/G_Q$ being the dimensionless zero-temperature conductance, in units of conductance quantum $G_Q = 2e^2/h$). The fluctuations increase, broadening

the distributions, as disorder is increased eventually driving a system through the localization-delocalization (LD) transition [5] at $g \sim 1$. Thus, the mesoscopic program was born where full distribution functions of relevant quantities in open (*e.g.*, conductance, local density of state, current relaxation times, etc.) or closed (*e.g.*, eigenfunction amplitudes, polarizability, level curvatures, etc.) samples are to be studied [1,6]. Especially interesting are the large deviations of their asymptotic tails from the ubiquitous Gaussian distributions (which can appear in mesoscopics only in the limit $g \to \infty$).

Recently, the study of fluctuations and correlations of eigenfunction amplitudes has been initiated [7]. The quantum coherence induces long-range spatial correlations (due to massless modes, like diffusons and cooperons) in the local density of states and eigenfunction amplitudes, which in turn lead to strong mesoscopic fluctuations of global quantities like conductance. Small deviations of eigenstate statistics from the universal predictions (applicable in the limit $g \to \infty$) of random matrix theory (RMT) are well

[a] *Present address:* Department of Physics and Astronomy, University of Delaware, Newark, DE 19716-2570.
e-mail: `bnikolic@physics.georgetown.edu`

understood through perturbative corrections $\sim \mathcal{O}(g^{-1})$ of the weak localization (WL) type [8], but the physical origin of large deviations in the far asymptotic tail of the distribution function is much more controversial [9–11]. Not only that there are different analytical predictions for the far tail asymptotics (which in fact do not explain all details of the tails found in numerical simulations [12,13]), but there is also an issue [11] of the relevant physics which is responsible for large wave function amplitudes (quantum *vs.* semiclassical) and a closely related question on the limitations of usually employed field-theoretical approaches [14] to study the disordered electron problem. Also, the parameters of the WL correction to the RMT framework cannot be explained (*e.g.*, in the Anderson model [13]) solely by the standard universal (independent of the details of disorder) quantities extracted from the semiclassical diffusive dynamics [7]. Instead, careful examination of ballistic effects, generated by the properties of particle dynamics on the length scale below the mean free path ℓ, is required [15]. Moreover, it is possible that some types of disorder could generate appreciable higher order terms (characterizing non-Gaussian features of random potential [16]) in this perturbative expansion in $1/g$, and thereby change the functional form of the perturbative correction as well. Thus, a detailed study of deviations from the RMT statistics in the paradigmatic case of a quantum particle in a random potential offers a possibility to unravel underlying correlations in a controlled fashion, which paves the way for understanding plethora of diverse problems (including those outside of physics [17]) where matrices containing random elements and their eigenstates are encountered.

In the course of exploration of mesoscopic fluctuations, the so-called prelocalized states have been unearthed as the microscopic origin of asymptotic tails of various distribution functions of thermodynamic and kinetic quantities [10,18–20]. While typical wave function is spread uniformly throughout a metallic sample of volume L^d with average amplitude $L^{-d/2}$ (up to inevitable Gaussian fluctuations), the prelocalized state in 3D exhibits much larger local amplitude splashes (on the top of the homogeneous background $|\Psi(\mathbf{r})|^2 \sim L^{-d}$) at some points $\mathbf{r}$ within the sample [7,13]. To obtain the far tail of such distribution "experimentally" (*e.g.*, in microwave cavities of Ref. [21] or by numerical simulations [13]) in "realistic" metallic systems, one has to search for extremely rare disorder configurations where quantum interference effects are able to generate highly unusual eigenfunctions.

What is the relevance of prelocalized states for transport experiments? Most of phenomena in good metallic disordered conductors are semiclassical in nature. This means that disorder-averaged properties, like conductance measured in experiments or calculated in (quantum transport) theory [22], are determined by the usual extended states of uniform amplitude, formed in the typical fluctuations of the random potential. However, recent experiments on quantum dots (nanofabricated samples with well-resolved electron energy levels) show that some transport properties, like fluctuations of the tunneling conduc-

tance, can depend sensitively on the local features of wave functions which couple the dot to external leads [23]. Also, to understand the excitation and addition spectra of quantum dots one has to deal with the statistics of Coulomb interaction matrix elements, which are influenced by the eigenfunction amplitude fluctuations [24]. By exploiting the correspondence between the Schrödinger and Maxwell equations in microwave cavities, it has become possible to probe directly the microscopic structure of wave functions in quantum disordered or quantum chaotic systems [21].

Here we undertake a comprehensive search, through numerical simulations, for special disorder configurations in order to investigate functional dependence of the parameters determining eigenstate statistics on the disorder strength or sample size. This is not just a 'brute force' study culminating in a fitting procedure of the observed distribution functions, but more importantly, an attempt to quantify those effects which can lead to substantial deviations from the RMT, departing even from the standard semiclassical corrections to it. Namely, our results stem from the exact solutions of the Schrödinger equation for a particle in a random potential, and therefore provide a reference point for the analytical approaches which usually integrate out some degrees of freedom by focusing on the "low energy" sector of a full theory [7]. For this purpose, we also compute exactly the transport properties of our finite-size samples, and relate them to the parameters extracted from the fits of analytical formulas to the perturbative and far tail intervals of the eigenfunction amplitudes. Mesoscopic physics intrinsically deals with finite-size phase-coherent samples, and has led to efficient use of different transport formalisms. Thus, we exploit the fact that transport properties of a specific sample (simulated here as nanoscale single band conductors) can be measured exactly on a computer. Although our focus is primarily on the peculiar states exhibiting the largest amplitudes (which generate far tails of the statistics of eigenfunction amplitudes, as well as of other mesoscopic quantities), it becomes necessary to investigate thoroughly the region of small eigenfunction amplitudes because of the possibility that the same semiclassical quantities (like classical diffusion propagator [25], which we evaluate explicitly for the samples with specific boundary conditions) might govern both portions of the distribution function [7].

We have investigated five different ensembles [26] of mesoscopic samples, each containing 30 000 weakly disordered three-dimensional (3D) metallic conductors. Finite-size samples are modeled by a tight-binding Hamiltonian (TBH)

$$\hat{H} = \sum_{\mathbf{m}} \varepsilon_{\mathbf{m}} |\mathbf{m}\rangle\langle\mathbf{m}| + \sum_{\langle\mathbf{m},\mathbf{n}\rangle} t_{\mathbf{mn}} |\mathbf{m}\rangle\langle\mathbf{n}|, \qquad (1)$$

with nearest-neighbor hopping $t_{\mathbf{mn}} = 1$ (unit of energy) between s-orbitals $\langle\mathbf{r}|\mathbf{m}\rangle = \psi(\mathbf{r} - \mathbf{m})$ located on sites $\mathbf{m}$ of a simple cubic lattice of size $L = 12a$ to $L = 20a$ (a is the lattice spacing). Periodic boundary conditions are chosen in all directions. The disorder is simulated by taking potential energy $\varepsilon_{\mathbf{m}}$ to be a uniformly distributed random variable, $-W/2 < \varepsilon_{\mathbf{m}} < W/2$, which is the
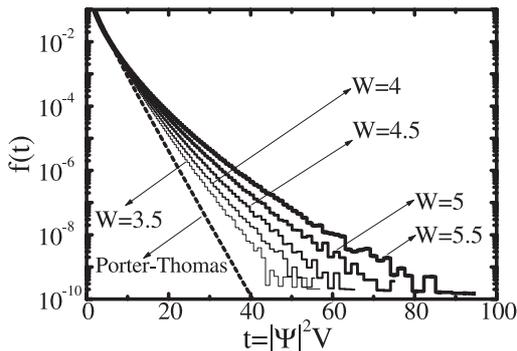
Fig. 1. Statistics of eigenfunction "intensities" $|\Psi_E(\mathbf{m})|^2$ in the band center $E \in (-0.15, 0.15)$ of an Anderson model on a simple cubic lattice 12^3. Each curve is obtained by examining about two million exact eigenstates of the (time-reversal and spin-rotation invariant) Hamiltonians whose on-site potential is a random variable uniformly distributed over the interval $[-W/2, W/2]$. The disorder strengths W for the five different sets of 30 000 Hamiltonians are chosen to ensure the diffusive ($L \gg \ell$) and semiclassical ($k_F\ell > 1$) transport regime in the conductors they model (relevant transport quantities are listed in Tab. 1.) The random matrix theory prediction for the limit $g \to \infty$ is Porter-Thomas distribution, plotted here as a reference.

Fig. 2. Comparison of the $W = 5$ eigenstate statistics $f(t)$ from Figure 1 for a lattice 12^3 and the statistics of band center eigenstates generated in the ensembles of 2000 or 500 conductors modeled on larger lattices 16^3 (with $\simeq 150$ eigenfunctions picked in a small energy interval $\Delta E = 0.3$ around $E = 0$ in each sample) or 20^3 (with $\simeq 300$ eigenfunctions investigated in each sample), respectively.

standard (Anderson) model in the localization theory [5]. The impurity configurations vary from sample to sample for a given disorder strength $W \in \{3.5, 4.0, 4.5, 5.0, 5.5\}$ which is chosen to ensure that ensemble-averaged transport quantities characterize metallic ($g \gg 1$) diffusive ($\ell \ll L$) transport regime at half filling (*i.e.*, at Fermi energy $E_F = 0$). For a weak $k_F\ell \gg 1$ (k_F is the Fermi wave vector) disorder, disorder-averaged transport properties are semiclassical, *i.e.*, well-described by the Bloch-Boltzmann formalism. Going beyond $W \simeq 6$ (but below critical $W_c \simeq 16.5$ for the localization of the whole band) would still give metallic conductance $g \gg 1$ (for large enough lattice), but the semiclassical concepts appearing in analytical predictions for the far tail [7], like ℓ, loose their meaning [22]. The disorder strengths below $W = 3$ are excluded only because of requiring too large lattices to avoid quasiballistic transport.

Statistical properties of eigenstates in a closed sample are described by a disorder-averaged distribution [10,25] of eigenfunction "intensities" $|\Psi_\alpha(\mathbf{r})|^2$

$$f(t) = \frac{1}{\rho(E)N} \left\langle \sum_{\mathbf{r},\alpha} \delta(t - |\Psi_\alpha(\mathbf{r})|^2 V)\delta(E - E_\alpha) \right\rangle, \quad (2)$$

on N discrete points $\mathbf{r}$ inside a sample of volume V. Here $\rho(E) = \langle \sum_\alpha \delta(E - E_\alpha) \rangle$ is the mean level density at energy E, and $\langle \dots \rangle$ denotes disorder-averaging. Normalization of eigenstates gives $\bar{t} = \int \mathrm{d}t\, t\, f(t) = 1$. We evaluate this function for eigenstates in the band center $E = 0$, which are obtained by exact numerical diagonalization of the Hamiltonian (1) [note that energy is a parameter in $f(t)$]. The distribution functions $f(t)$ for the five sets of conductors modeled on the lattice 12^3 is shown in Figure 1. The
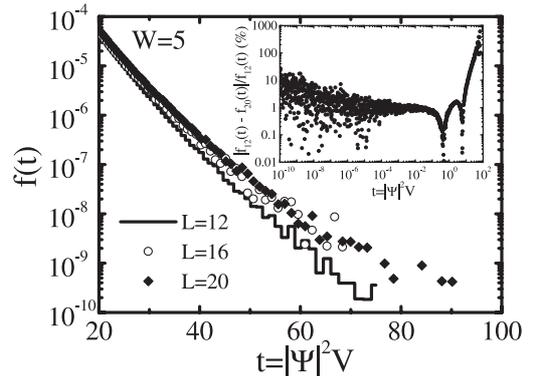
explicit dependence of $f(t)$ on the sample size is demonstrated in Figure 2 where $W = 5$ case is studied also on the 16^3 and 20^3 lattices. By searching through many configurations of the random potential one can find the rare ones which are responsible for the appearance of states with the highest possible amplitude splashes. We smooth out the data by additional averaging over a small energy interval (which taken alone, or combined with only a small number of disorder realizations, is not enough to study the prelocalized states), without introducing any artifact in the computed distribution functions [13]. This finally brings the number of analyzed eigenstates to about 2×10^6 for each curve plotted in Figure 1.

The rest of the paper is organized as follows. In Section 2 we provide a short survey of the main analytical results for the eigenstate statistics in 3D, which are expected to be relevant for our observations. Then in Section 3, a detailed comparison between these predictions, for both small and large deviations of distribution functions from RMT, and our results is undertaken using the calculated transport properties of the samples. Finally, we conclude in Section 4 by looking beyond the raw numbers and pointing out at open questions.

2 Statistical approaches to nonintegrable quantum systems

Quantum dynamics of a non-interacting particle in random potential (*e.g.*, generated by quenched impurities) has a long history of being a standard playground for the development of ideas of Anderson localization [5] and mesoscopic physics [2]. The classical counterpart of this problem is obviously chaotic, but it is only over the past two decades that its connections [14,28] to generic clean (*i.e.*, without stochastic disorder) examples of quantum

chaos [27] have been deepened. In both quantum chaotic and quantum disordered systems eigenstates are characterized solely by their energy, rather than by a set of quantum numbers. Since eigenstates and eigenvalues cannot be obtained analytically, it becomes useful to resort to some statistical treatment where one studies correlators averaged over large number of eigenstates instead of focusing on the properties of a single quantum state. Although the methods (and the language) of quantum chaos and quantum disorder have evolved independently, it was realized that Wigner-Dyson (WD) level statistics of RMT [28], a fingerprint [29,30] of quantum chaotic systems, is also applicable to disordered systems [14,31]. However, the lack of any transport-related energy or time scale in RMT description of the delocalized phase signals that relevant time to traverse the sample diffusively, $t_{\mathcal{D}} = L^2/\mathcal{D}$ ($\mathcal{D} = v_F \ell/3$ being the bare classical diffusion constant in 3D), is set to zero in this framework. Therefore, it became clear that WD statistics can be applicable to disordered system spectra only for the energy separation scale much smaller than the Thouless energy [32] $E_{\mathrm{Th}} = \hbar/t_{\mathcal{D}}$.

The physical origin of deviations from RMT in disordered systems with $g < \infty$ is the finite time $t_{\mathcal{D}}$ required for the particle to spread ergodically all over the sample, i.e., for the classical motion to explore the whole phase space. The statistical approaches to quantum disorder problems, like supersymmetric nonlinear σ-model (NLSM) [14] which maps stochastic problem to a field theory without randomness, provide the justification of RMT in the ergodic ($t \gg t_{\mathcal{D}}$) regime of diffusive dynamics. Furthermore, these techniques make it possible to study also the deviations from RMT for non-ergodic times or energy scales in weakly disordered ($k_F \ell \gg 1$) conductors—both perturbative and nonperturbative corrections are governed, within this framework, by the diffusion operator describing the dynamics of a corresponding classical system. The well-understood quantum chaotic properties of disordered system have made these systems a standard laboratory to test different approaches to generic quantum chaos [30,33] (where well-defined averaging procedure over an ensemble is lacking [34]). Thus, limitations of RMT encountered in disordered electron systems have put the study of deviations from the universality regime into the focus of both mesoscopic and quantum chaos communities [7,15], where "lessons from disordered metals" [35] have greatly influenced the development of formalism for more arduous examples of quantum chaos.

Recently, the equivalent program has been pursued for the eigenfunction statistics [7]. The earliest prediction for the (universal) distribution of eigenfunction intensities, in Gaussian orthogonal ensemble (GOE) of random matrices (which are time-reversal and spin-rotation invariant),

$$f_{\mathrm{PT}}(t) = \frac{1}{\sqrt{2\pi t}} \exp(-t/2) \qquad (3)$$

is known as the Porther-Thomas [37] (PT) distribution. Assuming only that eigenfunctions are normalized but otherwise arbitrary, $f_{\mathrm{PT}}(t)$ can be derived [38] from the probability that, e.g., component Ψ_1 [which corresponds to $\Psi(\mathbf{m}_0)$ at some point $\mathbf{m}_0$ inside the sample] of an eigenstate of a $N \times N$ random matrix is equal to some value t/N

$$f_{\mathrm{PT}}(t) = \lim_{N \to \infty} \frac{1}{N\sqrt{\pi}} \frac{\Gamma(N/2)}{\Gamma[(N-1)/2]}$$

$$\times \int_{-\infty}^{\infty} \left[\prod_{i=1}^{N} d\Psi_i \right] \delta(t - N|\Psi_1|^2) \, \delta\left(1 - \sum_{j=1}^{N} |\Psi_j|^2\right)$$

$$= \lim_{N \to \infty} \frac{1}{\sqrt{N\pi t}} \frac{\Gamma(N/2)}{\Gamma[(N-1)/2]} \left(1 - \frac{t}{N}\right)^{\frac{N-3}{2}}, \quad (4)$$

in the limit $N \to \infty$ (which corresponds to an infinitely large lattice in our problem). This is essentially an example of the central-limit theorem, and it should describe completely the eigenstate statistics in the universality limit that is insensitive to any physical details of the system. Such limit in disordered electron systems requires infinite conductance $g = E_{\mathrm{Th}}/\Delta \to \infty$ since level spacing Δ (thermodynamic scale) sets the smallest energy scale and $t_{\mathcal{D}} \to 0 \Leftrightarrow E_{\mathrm{Th}} \to \infty$ (in real systems E_{Th} is large only in small enough samples, such as quantum dots). The universality stems from the basis invariance of RMT, i.e., the fact that eigenfunctions in RMT are structureless with $\Psi_\alpha(\mathbf{r})$ and $\Psi_\alpha(\mathbf{r}')$ being uncorrelated for $|\mathbf{r} - \mathbf{r}'| \gtrsim \ell$, and fluctuating just as Gaussian random variables. However, random Hamiltonians of real disordered solids are tied to a real-space representation, where matrix elements are spatially dependent and TBH (1) is a band diagonal matrix. Therefore, they do not satisfy statistical assumptions of the standard RMT ensembles since all elements of such random matrices are non-zero and spatially independent. Nevertheless, a rigorous connection to the RMT eigenstate statistics (here just heuristically established through the interpretation of Eq. (4)) is provided by Efetov's supersymmetric approach [10,14] (i.e., zero-dimensional limit of the NLSM). While WD statistics works well for the part of spectrum contained within the interval $|E-E'| \ll E_{\mathrm{Th}}$, the distribution function $f(t)$ in finite g systems (like the ones in Fig. 1) do not overlap with PT distribution in any interval of eigenfunction amplitudes. The redistribution of amplitude statistics, caused in part by the appearance of highly unlikely according to RMT prelocalized states, leads to three different regions of intensities t. The deviations are the strongest in the large-t limit where $f(t)$ can be orders of magnitude greater than PT distribution. This occurs also in quantum chaos [39] where localization due to scars is generally less pronounced than inhomogeneities of the prelocalized states in strong enough disorder [21].

Small deviations of $f(t)$ from the PT distribution are accounted by a WL-type correction [8] (i.e., a quantity

sensitive to the breaking of time-reversal symmetry; here we use the expression for GOE)

$$f_{\mathrm{FM}}(t) = f_{\mathrm{PT}}(t) \left[1 + \frac{\kappa}{2} \left(\frac{3}{2} - 3t + \frac{t^2}{2} \right) + \mathcal{O}(g^{-2}) \right] \quad (5)$$

which is a regular function in the small parameter $1/g$ and can be derived by a perturbative treatment of the nonzero spatial modes of the NLSM. This result was obtained by Fyodorov and Mirlin [8] (FM) for $t \ll \kappa^{-1/2}$ (where correction is smaller than the RMT term). As in the case of corrections to WD statistics, the deviations are parameterized by the properties of classical diffusive dynamics. Namely, κ is defined in terms of the diffusion propagator (i.e., one-diffuson loop) [7]

$$\kappa_{\mathrm{diff}} \equiv \Pi(\mathbf{r}, \mathbf{r}) = \frac{2}{g\pi^2} \sum_{\mathbf{q}} \frac{\exp(-\mathcal{D}\mathbf{q}^2\tau)}{\mathbf{q}^2 L^2}, \quad (6)$$

which is the sum over the diffusion modes (diffusion propagator $\Pi(\mathbf{r}, \mathbf{r}')$ is the Green function of the diffusion equation and can be expressed in terms of eigenvectors and eigenvalues of the diffusion operator $-\mathcal{D}\mathbf{q}^2$, in a rectangular geometry studied here). The sum in equation (6) diverges linearly in 3D at large momenta, thus requiring a cutoff at $|\mathbf{q}| \sim 1/\ell$ to retain the validity of the diffusive approximation. We provide the ultraviolet regularization using exponential damping factor [41] which limits the sum to the diffusive regime $\mathcal{D}\mathbf{q}^2 \ll 1/\tau$ ($\tau = \ell/v_F$ is the elastic mean free time)

$$S(y) = \frac{1}{4} \sum_{n_x, n_y, n_z \neq 0} \frac{\exp[-4\pi^2(n_x^2 + n_y^2 + n_z^2)\, y]}{n_x^2 + n_y^2 + n_z^2} . \quad (7)$$

Here the wave vectors $\mathbf{q}$ are quantized by the periodic boundary conditions used in all directions, $q_x = 2\pi n_x/L$, $n_x = \pm 1, \pm 2, \ldots$, and correspondingly for q_y and q_z. The argument y is expressed in terms of the semiclassical transport quantities

$$y = \frac{\mathcal{D}\tau}{L^2} = \frac{1}{3} \left(\frac{\ell}{L} \right)^2. \quad (8)$$

The sum (7) can be evaluated exactly by a simple numerical computation. On the other hand, its analytical dependence on ℓ/L is usually obtained after approximating the discrete summation by an integral (a standard result in the literature is therefore quoted [8] as $S(y) \sim L/\ell$). To avoid loosing the terms of the original sum, which depend on specific boundary conditions [41], it is necessary to evaluate the original discrete form. Following reference [41] this can be done by using the function $F(y) = \sum_{n=1}^{\infty} \exp(-\pi^2 n^2 y)$,

$$\frac{\partial S(y)}{\partial y} = -\pi^2 [2F(4y)]^3. \quad (9)$$

Since $F(y)$ is related to the complete elliptic integrals, for small values of argument $y \ll 1$ they can be approximated

by the leading order to give

$$F(y) \simeq \frac{1}{2} \left[(\pi y)^{-\frac{1}{2}} - 1 \right], \quad (10)$$

which, upon integration in (9), leads to

$$S(y) = \frac{\sqrt{\pi}}{4\sqrt{y}} + \frac{3}{4}\,\pi\,\ln(y) - 3\,\pi^{3/2}\,\sqrt{y} + \pi^2 y + \alpha_P. \quad (11)$$

The integration constant α_P can be fixed numerically by finding the limit, as $y \to 0$, of the difference between exactly calculated discrete sum $S(y)$ and its analytical approximation (11) with removed constant α_P. We find that this difference converges at small $y < 10^{-4}$ to $\alpha_P \approx 8.32$. For the largest ℓ in our study, the function (11) with this α_P reproduces the numerically calculated sum over the diffusion modes to within 2%. Evaluation of $S(y)$ in the standard way, by approximating it with an integral, gives only the leading term (which is the same for all boundary conditions)

$$S_I(y) = \frac{\sqrt{\pi}}{4\sqrt{y}} - \alpha_I, \quad (12)$$

where α_I is an integration constant defined by the infrared cutoff at small wave vectors $|\mathbf{q}| \sim L^{-1}$.

The divergence of the sum over diffusion modes (7) in 3D points out that more careful treatment is needed of the short-scale physics. Since κ has the meaning of a time-integrated return probability for a diffusive particle [7], it can be generalized to the ballistic case (various transport and thermodynamic phenomena encountered in disordered conductors are related to the classical return probabilities for a diffusive particle, see Ref. [45]). Using ballistic generalization [42] of the NLSM to go beyond the diffusive approximation, it was shown [7,15] that corresponding ballistic contribution to this return probability, i.e., the probability for a particle to be scattered only once from an impurity and return back after a time $t \ll \tau$, has to be added to κ_{diff}. Therefore, the total return probability is expected to be given by $\kappa = \kappa_{\mathrm{diff}} + \kappa_{\mathrm{bal}}$. Such (semiclassical) ballistic effects are non-universal, i.e., they can depend strongly on the microscopic details of disorder (they are negligible in the case of smooth potential having a correlation length much bigger than $1/k_F$ [7,43]). In fact, it was shown recently [13] that κ_{bal} determining perturbative corrections in the Anderson model can be much greater than κ_{diff}. In Section 3 we show explicitly that both contributions are needed to describe κ as a function of disorder strength, contrary to some previously reported results [44] for the 3D Anderson model where fitted κ was related to ballistic effects only.

The second point of intersection of computed distribution function with PT distribution can be considered as the point at which a tail of $f(t)$ starts to form. While $f_{\mathrm{FM}}(t)$ still approximately describes the "near tail" around these values of t, the slow decay of $f(t)$ eventually requires a nonperturbative formula in $1/g$. Such is provided by the 3D case calculations [46] in the framework of

standard diffusive NLSM, which give with an exponential accuracy

$$f_{\text{NLSM}}(t) \sim \exp\left[-\frac{1}{4\kappa}\ln^3(\kappa t)\right], \ t \gtrsim \kappa^{-1}, \qquad (13)$$

and stems from the appearance of the prelocalized states. Since $\kappa \sim (k_F\ell)^{-2}$ (only in the leading order—the discrete sum in equation (7) also contains other terms), this result written down to the leading order term of the cubic polynomial in $\ln[t/(k_F\ell)^2]$,

$$-\ln f_{\text{NLSM}}(t) \sim (k_F\ell)^2 \ln^3\left[\frac{t}{(k_F\ell)^2}\right], \qquad (14)$$

emphasizes that prefactor contains $(k_F\ell)^2$ dependence on the disorder strength. However, the numerical constant is uncertain [46] because of being determined by the ultraviolet $\mathbf{q}$ (in the field theoretical language), i.e., length scales $\lesssim \ell$ which are outside of the diffusive NLSM framework. Namely, the standard nonlinear σ-models [14,18] are long-wavelength effective field theories for the diffusive modes whose saddle point is analyzed to get the eigenstate statics [10,19,46]. The role of energy is played by the diffusion operator $-\mathcal{D}\nabla^2$, so that fundamental variables of the theory, $Q(\mathbf{r})$ matrix fields, should vary spatially on the scale much larger than ℓ. However, it was found [10,46] that in 3D systems $Q(\mathbf{r})$ vary rapidly on the length scale $\sim \ell$, which then impedes the prospect of getting rigorous results and points out to a different physics determining the structure of eigenfunctions in 3D, than is the case if low-dimensional systems [7,12]. An attempt to overcome this limitations, by using ballistic NLSM which extends the semiclassical description to all momenta $|\mathbf{q}| \lesssim k_F$, leads to the same $(k_F\ell)^2$ prefactor dependence but offers $\pi/9\sqrt{3}$ as the precise value of its constant piece [47].

In between the perturbative ($t \ll \kappa^{-1/2}$) and the far-tail region ($t > \kappa^{-1}$) of the wave function amplitudes, NLSM analysis of $f(t)$ predicts an intermediate range of amplitudes, described by [10]

$$f_{\text{IM}}(t) \simeq \frac{1}{\sqrt{2\pi t}} \exp\left[\frac{1}{2}\left(-t + \frac{\kappa t^2}{2} + \cdots\right)\right],$$
$$\kappa^{-1/2} \lesssim t \lesssim \kappa^{-1}. \qquad (15)$$

This has also has the form of the corrected PT distribution, as is the case of FM distribution. However, the correction term here is in the exponent, and therefore of a different type than the one in $f_{\text{FM}}(t)$. It should be large compared to unity, but small compared to the leading RMT term [7].

An alternate route to account for the slow decay of $f(t)$ at large amplitudes has been undertaken through a "direct optimal fluctuation method" (DOF) of reference [11]. This approach suggests possible importance of ballistic non-semiclassical effects, which are missed in both diffusive and ballistic NLSM formulation, by analyzing the short-scale structure of solutions of the Schrödinger equation (i.e., by analyzing the saddle point of the original problem

of quantum particle in a random potential, rather than the saddle point of its effective field theory obtained by integrating out the disorder degrees of freedom). It gives the following result for the far tail asymptotics (where only the leading log-cube term of the full cubic polynomial of $\ln t$ is computed explicitly)

$$f_{\text{DOF}}(t) \sim \exp\left[-C_{\text{DOF}}\, k_F\ell \ln^3 t\right], \qquad (16)$$

assuming Gaussian white-noise random potential, and estimating $C_{\text{DOF}} \simeq 3 \times 10^{-3}$ for that type of disorder. The dependence on the prefactor on $k_F\ell$ here is linear, which can substantially increase the probability to observe a rare event as compared to NLSM prediction. Nonetheless, this result has also been interpreted heuristically within the NLSM picture [7], assuming that κ might depend solely on the non-universal (semiclassical) ballistic $\sim 1/k_F\ell$ contributions of the same kind as those encountered in the region of small eigenfunction amplitudes.

3 Fitting the eigenstate statistics: physics behind deviations from random matrix theory

In this section, we first describe the details of the computation of $f(t)$, and also give elementary account of the quantum transport properties of conductors described by the Anderson model. This should serve as an overture for the subsequent detailed examination of the eigenstate statistics in the perturbative region (i.e., the main body of the distribution function of intensities), and nonperturbative region (where amplitude splashes generate large deviation from PT distribution), by attempting to fit the analytical forms introduced in Section 2. We then analyze the confidence in such descriptions through relative error of the corresponding fits. The extracted fitting parameters are interpreted by comparing them to the expected ones in the analytical predictions, with the help of transport properties of our finite-size samples.

We solve exactly the eigenproblem of the TBH (1) of a finite-size system inside a small energy window $\Delta E = 0.3$ positioned around $E = 0$. This interval picks 60–70 states in each of the 30 000 conductors (modeled on the lattice 12^3) with different impurity configurations. The ensemble of disordered samples is characterized by the disorder-averaged conductance g. The overall number of collected states depends on disorder—as the disorder is increased the energy band broadens, meaning that some states start to appear with energy eigenvalues beyond the band edge $E_b = 6t$ of the clean TBH while the average number of states in the band center decreases. These states are used to evaluate $f(t)$ as a histogram of intensities at all points inside the sample ($N = 12^3$). The two delta functions in equation (2) are approximated by box functions $\bar{\delta}(x)$. The width $\Delta E = 0.3$ of $\bar{\delta}(E)$ is such that $\rho(E)$ is constant inside ΔE. The amplitudes of wave functions are sorted in the bins defined by $\bar{\delta}(t - |\Psi_\alpha(\mathbf{r})|^2 V)$, where their width is constant on a logarithmic scale.

As emphasized in Section 1, before embarking on the search for prelocalized states, we first compute the

Table 1. Transport properties computed for our five ensembles of impurity configurations characterized by different diagonal disorder strength W in the Anderson model on a simple cubic lattice 12^3.

	g	ℓ (a)	κ_{diff}
$W = 3.5$	21.5	2.89	0.00074
$W = 4.0$	17.4	2.21	0.0031
$W = 4.5$	14.3	1.75	0.0084
$W = 5.0$	11.9	1.42	0.018
$W = 5.5$	10.0	1.17	0.035

transport properties of our samples. The exact zero-temperature conductance of the nanoscale finite-size sample is obtained from the Landauer-type formula [48]

$$g = \mathrm{Tr}\left[\mathbf{t}(E_F)\mathbf{t}^\dagger(E_F)\right], \quad (17)$$

where transmission matrix $\mathbf{t}(E_F)$ is expressed in terms of the real-space Green functions [49] for the sample attached to two disorder-free semi-infinite leads. The details of such calculations for the lattice model studied here are given elsewhere [22]. Here we just clarify the relationship of this conductance to the Thouless conductance $g_{\mathrm{Th}} = 2\pi E_{\mathrm{Th}}/\Delta$ (expressed in terms of the spectral properties of a closed sample), which appears in standard analytical treatments of various disordered problems, including the eigenstate statistics [7]. This mesoscopic computational technique opens the sample to the surrounding ideally conducting medium, so that particles can leave and enter through the lead-sample interface. Thus, the discrete levels of an initially isolated sample are smeared, and spectrum of *sample+leads=infinite system* becomes continuous (which allows us to find the conductance at any E_F inside the band). However, the computed conductance, for not too small disorder [50,51] or coupling to the leads of the same transverse width as the sample [50], is practically equal to the "intrinsic" conductance g_{Th}. In practice this means that we attach sample to the leads of the same cross section and use the same hopping matrix element $t_{\mathbf{mn}}$ throughout the system (*i.e.*, in the leads, lead-sample coupling and in the sample), in order to minimize any influence which leads can have on the conductance [51].

The disorder-averaged transport quantities, characterizing the five ensembles of conductors studied here, are listed in Table 1. For weak disorder $W \lesssim 6$ conductance g is dominated by the semiclassical effects [22]. Thus, we use the Bloch-Boltzmann formalism (applicable when $\ell \gg a$ [22]), in Born approximation for the scattering on a single impurity, to get the elastic mean free path $\ell(E_F = 0) \simeq 35.4/W^2$ shown in Table 1. Analytical treatments usually assume a simple spherical Fermi surface for which k_F is just the radius of the sphere. Such quantity is not well-defined for a lattice system with non-spherical Fermi surface where k_F is direction dependent (*i.e.*, different average values can be obtained depending on whether one averages the absolute value of k_F or the root-mean-square of k_F over the Fermi surface). Nevertheless, all dif-
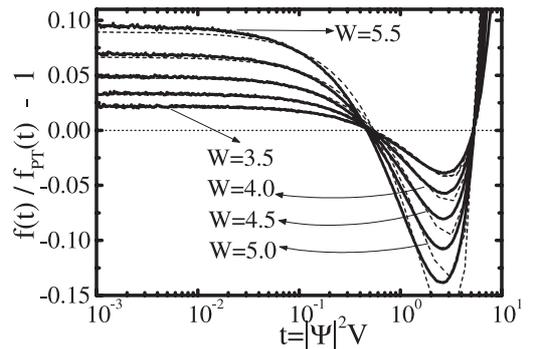

Fig. 3. Weak localization correction $\kappa/2\,[3/2 - 3t + t^2/2]$, through which $f_{\mathrm{FM}}(t)$ accounts for the small deviations from the Porter-Thomas distribution $f_{\mathrm{PT}}(t)$, fitted (dashed lines) to $f(t)/f_{\mathrm{PT}} - 1$ in the perturbative region of amplitudes for statistics from Figure 1. The first zero of all curves is W dependent and falls in the interval (0.46,0.51); the second one is at ≈ 0.53. This should be compared to the two zeros $t_0' = 0.55$ and $t_0'' = 5.45$ of $3/2 - 3t + t^2/2$. This fit is expected to be valid from $t < 1/\sqrt{\kappa}$ to $t = 0$—we find the relative error $[f(t) - f_{\mathrm{FM}}(t)]/f(t)$ to be less than 1% all the way to $t \sim 10^{-11}$ (up to some noise in the data at the smallest investigated t).

ferent averaging procedures give similar values, and we use conventionally the one which would reproduce some transport formula, like Sharvin [52] classical point contact conductance $G = G_Q\,k_F^2 L^2/4\pi$, where such average values (here over the Fermi surface $E_F = 0$ of a simple cubic lattice) naturally appear. This convention gives $k_F \approx 2.8/a$, which should serve as a counterpart of k_F appearing in theoretical simplifications assuming Fermi sphere. It is easy to check that these values of parameters, plugged into the Drude-Boltzmann formula $g \simeq (k_F^2 L^2/4\pi)\,(\ell/L)$, approximately reproduce the disorder-averaged Landauer two-probe conductances from Table 1.

3.1 Perturbative deviations from the RMT limit

We commence the comparison between our results in Figure 1 and functional forms from Section 2 by fitting FM distribution (5) to the data in the region of amplitudes where $f(t)$ deviates only slightly from PT distribution. The plot of $f(t)/f_{\mathrm{PT}}(t) - 1$ (Fig. 3) offers a straightforward way to check for the non-trivial feature of the correction term, such as whether the zeros $t_0' = 0.55$ and $t_0'' = 5.45$ of $3/2 - 3t + t^2/2$ are exhibited by our data. We find that zeroes of the curves from our numerical simulation are slightly smaller (Fig. 3), the first one being even disorder strength dependent. Since naive (visual) inspection of fits, especially on a logarithmic scale might lead to erroneous conclusions (like the range of amplitudes where some function fits the data), we establish a quantitative criterion of the quality of a fit with some formula $f_{\mathrm{fit}}(t)$ by looking at the relative error $[f(t) - f_{\mathrm{fit}}(t)]/f(t)$. This becomes especially important in assessing the fit of the far tail on the semilogarithmic scale (an example of such assessment is shown in Fig. 7). Moreover, this type of plot
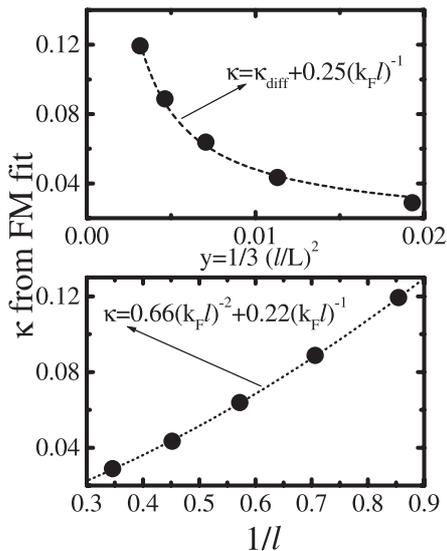
Fig. 4. The extracted κ from the fits of FM distribution (Fig. 3) to the portion of our numerical distribution $f(t)$ contained within the interval of t where deviations from the Porter-Thomas distribution of RMT are small. The dependence of these values on the disorder strength (*i.e.*, mean free path ℓ) is explained as a sum of the diffusive contribution $\sim 1/(k_F\ell)^2$ (or, more precisely, k_{diff} expressed through the full sum (11), as shown in the upper panel) and the ballistic contribution $\sim 1/k_F\ell$.

directly highlights intervals where some analytical formula can be considered to describe the data. For example, this gives a quantitative insight into the boundaries of perturbative, intermediate and nonperturbative regions discussed in Section 2. The FM distribution describes $f(t)$ for small eigenfunction amplitudes completely in the weakly disordered samples, where $[f(t) - f_{\mathrm{FM}}(t)]/f(t)$ is less than 1% for the data and the fit in Figure 3. It also fits the statistics in the conductors where dirty metal regime of transport is reached in the Anderson model (*e.g.*, the resistivity of $W = 5.5$ sample would be $\simeq 500\,\mu\Omega$cm for lattice spacing $a = 3$ Å). However, it is demonstrated by Figure 3 that increasing W toward the boundary $W \simeq 6$ leads to larger relative difference between the fitted FM distribution function and the numerical data, while also shrinking the interval of t where such comparison is still reasonable in the first place. For $W \gtrsim 6$ unwarranted application of the Drude-Boltzmann formula would give $\ell < a$ (*i.e.*, the transport in this regime is dominated by non-semiclassical and nonperturbative effects [22]). Therefore, even though it might be possible to claim that FM form accounts for some portion of $f(t)$ at stronger disorder [44], the direct comparison of extracted parameter κ to the calculated one becomes nonsensical. For example, W cannot be interpreted as $\sim \ell^{-1/2}$ in this regime. In fact, the departure of FM correction from our $f(t)$ starts before the upper limit of disorder, determining the breakdown of Bloch-Boltzmann theory of semiclassical transport, is reached. Similar distinction between the disorder limitation for the diagrammatic results and somewhat higher

limit for the validity of Boltzmann equation is seen in some other cases [53] (despite the fact that Boltzmann theory is rigorously justified as a lowest order result of a perturbative expansion of *e.g.*, the Kubo formula).

The one-parameter fit of the FM result equation (5) allows us to extract the first relevant physical parameter from our data, κ. The extracted values are presented in Figure 4. These values of κ do not match to the calculated κ_{diff} (Tab. 1) determined by the universal properties of the diffusive dynamics. This is not surprising in the light of the discussion in Section 2. What might be surprising is that disorder-specific $\kappa_{\mathrm{bal}} = \kappa - \kappa_{\mathrm{diff}}$ can be few times greater than κ_{diff}. This points out to the importance of the short-scale effects even in the perturbative region. Nevertheless, it appears that non-Gaussian features (non-zero higher order cumulants) of the uniformly distributed random potential of the Anderson model do not generate interesting terms beyond the second-order ones computed explicitly in the FM correction.

For a system of fixed size, Figure 4 shows that κ changes with the strength of disorder in a way expected for the change of a sum of the two contributions. The first term in the phenomenological formula for $\kappa = 0.66(k_F\ell)^{-2} + 0.22(k_F\ell)^{-1}$ is different from the analytically computed κ_{diff}. However, the function fitting the data on the lower panel of Figure 4 is only the leading order behavior (usually given when boundary conditions quantizing the diffusion modes are neglected [41]) of the full κ_{diff} computed in Section 2. Therefore, we proceed to fit formula (6) in the following form

$$\kappa = \frac{K_1}{\sqrt{y}}\frac{2S(y)}{\pi^2} + \frac{K_2}{\sqrt{y}}\,. \qquad (18)$$

That such fit of κ *vs.* $y = 1/3(\ell/L)^2$ is successful is shown on the upper panel of Figure 4, and also by comparing $K_1/\sqrt{y} = 0.012L/\ell$ factor in the first term to the expected $1/g = (4\pi/k_F^2L^2)(L/\ell) = 0.011$. The remarkably close numerical values confirm suggest that $\kappa_{\mathrm{diff}} + 0.23(k_F\ell)^{-1}$ should include the lower order boundary condition dependent terms [41] in κ_{diff}. While it would be hard to investigate this extra terms from the scaling of numerically computed disorder-averaged conductance (because of "pollution" by the conductance fluctuations), here they parameterize the features of mesoscopic fluctuations themselves.

The other important question concerns with the dependence of the two contributions on the sample size. Standard display of κ_{diff} and κ_{bal} in the literature shows only the leading order terms of such parameters, like equation (14) or equation (16), which are L-independent [7,11]. The short-scale contributions to κ are not sensitive to the sample boundaries, so that change of the fitted κ in $f_{\mathrm{FM}}(t)$ with L should be generated solely by a change of $\kappa_{\mathrm{diff}}(L)$. Our evaluation of κ_{diff} introduces several size dependent terms, cumulative effect of which is shown in the upper panel of Figure 5. In the limit of large system size, this converges asymptotically to $\lim_{L\to\infty}\kappa_{\mathrm{diff}}(L) = 0.11$. This offers a simple test of the accuracy of the regularization scheme employed to obtain $\kappa_{\mathrm{diff}}(L)$. In order to
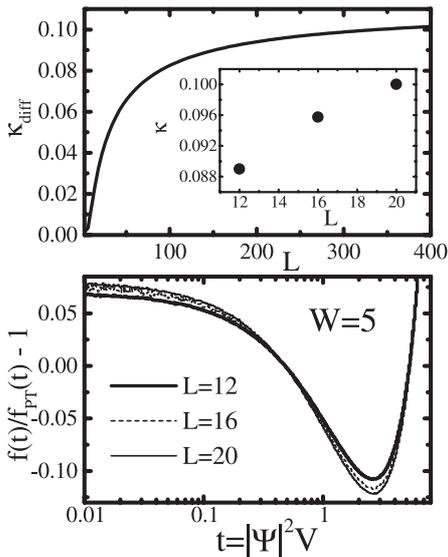
Fig. 6. Exp-log-cube fits, equations (19) and (20), *versus* attempted log-normal fit to the far tail of $f(t)$ for $W = 5$ ensemble of disordered conductors from Figure 1. The numerical data for our three-dimensional systems clearly favor exp-log-cube asymptotics. Relative error of the fits is plotted in Figure 7.

Fig. 5. The region of small deviations of $f(t)$ from the RMT statistics $f_{\mathrm{PT}}(t)$ in the three sets of $W = 5$ disordered conductors (lower panel), which differ by the lattice size: 12^3, 16^3 and 20^3 (Fig. 2). Fitting WL correction $\kappa/2\,[3/2 - 3t + t^2/2]$ to these curves gives κ as a function of L, as shown in the inset of the upper panel. This should be compared to size-dependence of its diffusive contribution κ_{diff} in equation (6), since ballistic contributions are size independent.

investigate this issue, we generate a set of conductors modeled on the lattices 16^3 and 20^3 with $W = 5$ disorder strength. The comparison between the corresponding distributions $f(t)$ is shown in Figure 2; using the same energy window $\Delta E = 0.3$, this distributions are generated from about $\simeq 150$ or $\simeq 300$ states, for each realization of disorder, which are picked in the band center of 16^3 or 20^3 lattice, respectively. Even without too large statistics, a palpable deviation between the two distributions is observed in the far tail, and also in the region of small t. In quantitative terms, analytical expression (6) gives $\kappa_{\mathrm{diff}}(L = 12) = 0.019$, $\kappa_{\mathrm{diff}}(L = 16) = 0.028$, and $\kappa_{\mathrm{diff}}(L = 20) = 0.036$, while the fitted ones are $\kappa(L = 12) = 0.089$, $\kappa(L = 16) = 0.096$ and $\kappa(L = 20) = 0.100$. At lower disorder $W = 3.5$ we get somewhat better agreement between fitted and calculated change in κ with the system size: $\kappa(L = 20) - \kappa(L = 16) = 0.0036$ *versus* $\kappa_{\mathrm{diff}}(L = 20) - \kappa_{\mathrm{diff}}(L = 16) = 0.0027$, in accord with the discussion above on the disorder strength boundaries for the validity of perturbation theory in $1/k_F\ell$.

3.2 Far tail

A common feature of (almost) all analytical results for the eigenstate statistics in 3D metallic samples is that some exp-log-cube formula is predicted to describe the large-t asymptotic behavior of $f(t)$. Thus, the most general functional form along these lines would be an exponent of a cubic polynomial of $\ln t$. Since lower order terms in the
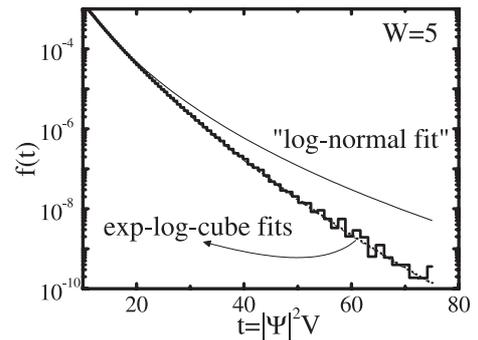
polynomial are rarely calculated, and fitting of any formula is more reliable when the number of free parameters is small, we choose to fit two different simple (employing only two parameters) exp-log-cube expressions (postponing the physical interpretation of their parameters for a moment):

$$f_{\mathrm{fit}}(t) = C_p \exp(-C_3 \ln^3 t), \qquad (19)$$

which is always the leading order term (and sometimes the only one amenable to explicit computation, like in Eq. (16)), and the NLSM-like result (13)

$$f'_{\mathrm{fit}}(t) = C'_p \exp\left[-\frac{1}{4\kappa_{\mathrm{ELC}}} \ln^3(\kappa_{\mathrm{ELC}} t) \right]. \qquad (20)$$

Using the fitted κ from Figure 4, we first establish the boundaries of different intervals for $f(t)$ which are discussed in Section 2 (*e.g.*, according to equation (13) the beginning of the far tails is approximately located at $t \gtrsim 1/\kappa$). These serves as a consistent criterion, where portion of $f(t)$ to be fitted with exp-log-cube formula analytical enlarges with increasing W, thus avoiding spurious results when attempting to fit too large piece of the distribution function. Although log-normal asymptotics is expected in 2D systems [7,11] (and has been confirmed numerically [12]) it has also appeared as a candidate in 3D systems [10]. However, attempt to fit $C''_p \exp(-C_2 \ln^2 t)$ to our data fails completely, as shown in Figures 6 and 7.

To check quantitatively the level at which fitted exp-log-cube formulas match $f(t)$ from the numerical simulation, we perform our stringent test by plotting the relative error in Figure 7. The possibility to fit both functions (13) and (20) in a more or less similar way is shown in Figures 6 and 7. Thus, a portion of $f(t)$ can be well-described by the exp-log-cube asymptotics, where the size of the interval of amplitudes where the relative error is small (because of the noise in the data points of $f(t)$ being pushed to the largest values of t) increases with increasing disorder strength. Another conclusion which can be drawn from Figure 7
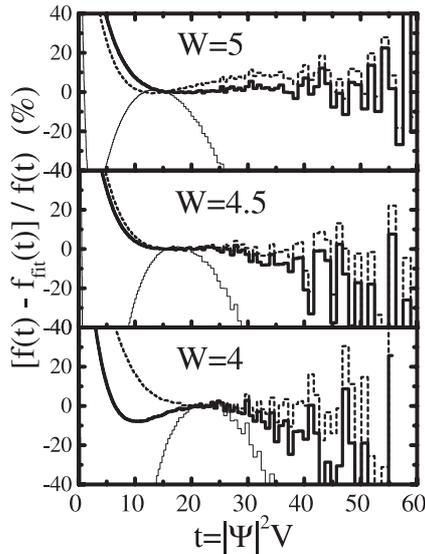
Fig. 7. Relative error of the two different ways of fitting the exp-log-cube formula (as well as the illustration of inadequacy of the "log-normal fit" from Figure 6, thin solid line) to the exact $f(t)$ from Figure 1: thick solid line is for $f_{\rm fit}(t) \equiv C_p \exp(-C_3 \ln^3 t)$ and dashed line is for $f'_{\rm fit}(t) \equiv C'_p \exp[-1/4\kappa_{\rm ELC} \ln^3(\kappa_{\rm ELC}t)]$.
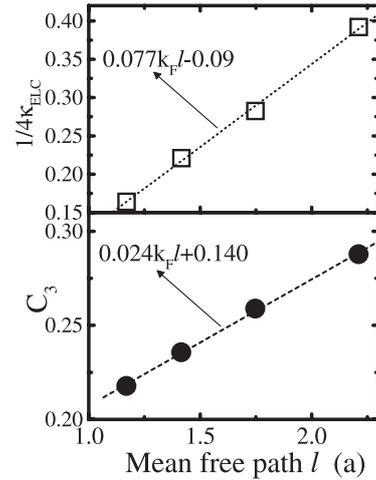

Fig. 8. Parameters of the two different exp-log-cube formulas (see Eqs. (19, 20)), fitted to the far tail of $f(t)$ in Figure 1, as a function of disorder strength (measured by ℓ). The success of the linear fitting of both C_3 and $1/4\kappa_{\rm ELC}$ vs. $k_F\ell$ favors analytical predictions having first power of $k_F\ell$ as the prefactor of the leading log-cube order, thereby supporting DOF conclusions [11] which emphasize that short-scale effects govern the far tail in 3D systems.

is that a narrow intermediate region of amplitudes exists which is not covered by either the FM function or exp-log-cube asymptotics. However, it appears that it cannot be fitted at all by the intermediate formula (15), which is too akin to the PT distribution for this to work here.

We now proceed by analyzing dependence of the extracted parameters on the disorder strength $k_F\ell$, as well as by looking at the consequence of interpreting $\kappa_{\rm ELC}$ to have the same physical meaning as κ obtained by fitting the FM formula to the perturbative region (Fig. 3). This interpretation is in the spirit of NLSM conclusions where both perturbative and nonperturbative corrections to RMT eigenlevel or eigenstate statistics are governed by the same semiclassical physics [7]. However, their values turn out to be quite different along the respective portions of $f(t)$. The most important finding in the far tail is that both prefactors C_3 and $1/4\kappa_{\rm ELC}$ appear to increase linearly with $k_F\ell$, as shown in Figure 8. Since prefactors are the most conspicuous signature of the importance of underlying ballistic or diffusive effects, this would mean that ballistic effects completely dominate in the far tail (explaining *e.g.*, why we find $\kappa_{\rm ELC} \gg \kappa > \kappa_{\rm diff}$) and confirming the conclusions of DOF analysis [11] where short-scale structure of the solutions of Schrödinger equation is pointed out to be solely responsible for the rare events at the largest possible intensities t. Nevertheless, a puzzle remains: both prefactors depend on the sample size (which is not treated explicitly in the present analytical schemes [7,11]), whereas it is plausible that ballistic effects are insensitive to L. For example, at $W = 5$ we have to use $C_3 = 0.218$ or $\kappa_{\rm ELC} = 1.411$ (compare with corresponding values in Fig. 8) to fit the far tail of $f(t)$ in Figure 2 for

the sample of size $L = 20a$. This suggests that a theory is needed where such size-dependent effects are handled explicitly (their magnitude cannot be explained by, *e.g.*, the change in $\kappa_{\rm diff}(L)$ as is approximately possible for the size dependence of parameters in the small-t region).

4 Conclusions

Our results confirm that statistical distribution of eigenfunction amplitudes in 3D mesoscopic disordered systems depends crucially on short-scale ballistic effects (and thereby on the details of a random potential). In fact, the exactly computed universal quantities characterizing the classical diffusion process generate much smaller contribution to the parameters needed to describe the observed distributions by the analytically predicted formulas. This is revealed in the perturbative region of amplitudes, where deviations of the eigenfunction amplitudes distribution function from the RMT limit are small, and Fyodorov-Mirlin distribution (*i.e.*, Porter-Thomas distribution corrected by the weak localization terms) captures their functional form for weak enough disorder (*i.e.*, the upper limit of disorder strength should be smaller than the one determining the breakdown of other semiclassical properties, like Drude-Boltzmann conductance) in the Anderson model of localization. In this interval of small eigenfunction amplitudes, the diffusive contribution contains boundary conditions dependent weak localization terms, which stem from evaluation of the discrete sum over the diffusion modes. In the region of large wave function amplitudes, deviation from the RMT appears in the form of far tail of the distributions function, and is governed by the prelocalized states formed in rare configurations

of the random potential. The far tail, which we obtain after examining about 2×10^6 exact eigenstates, cannot be accounted by the log-normal distribution, but is well-described by the exp-log-cube formulas. However, substantially different parameters, used in NLSM formalism with clear physical interpretation, are needed for this when compared to the ones governing the small deviations. Nevertheless, their linear dependence on the disorder strength (measured by $k_F\ell$) is in accord with prefactor of the DOF theory, where short-scale effects were pointed for the first time as the possible sole explanation of the far tail statistics (we cannot decipher whether these effects are of semiclassical or genuine quantum origin). These findings appear to be quite different from the success of various semiclassically based theories [54] in describing the spectral statistics in mesoscopic systems, which are dominated by the general properties of quantum coherent superpositions and diffusion. The problems with standard diffusive semiclassical description appear in the study of statistics of any quantity where corrections to RMT are expressed in terms of the sums which diverge above some specific space dimensionality [20] (such as $d \geq 2$ in the eigenstate statistics problem). Our analysis points out that regularization schemes, which *ad hoc* avoid divergences from the short-length scales below ℓ by introducing a cutoff at large momenta $|\mathbf{q}| \sim 1/\ell$, can lead to large discrepancies when compared to exact numerical results.

The feature of the far tails in the Anderson model which does not fit into the picture of ballistic effects alone is the need for specific prefactors terms which can account for the observed size dependence of the statistics. One possible explanation for these discrepancies would be the lattice effects in our model, but real solids are lattice structures (here simplified by taking single orbital per site) and possibility of such effects would not be an artifact of the model (which has been a paradigmatic model of the localization theory since the seminal paper of Anderson [5]). The other possibility stems from the fact that, even though our samples are good metals with $g > 10$, they are not large enough to be in the vicinity $g \gg 1$ of universality limit, which is the region treated by present theories. Strictly speaking, our findings can be considered as a demonstration of the structure of eigenfunctions in nanoscale conductors, and to contrast their structure to the predicted one in the limit $g \gg 1$, a heuristic attempt to account for the small-size corrections might be useful. Thus, if we interpret $t = |\Psi(\mathbf{r})|^2 V$ of the standard statistical analysis as the ratio of eigenfunction intensity to its typical value $1/V$ far away from the high amplitude splashes, then by the same token, in small samples we can construct statistics of analogous quantity $t' = |\Psi(\mathbf{r})|^2/|\Psi(\mathbf{r})|^2_{\mathrm{typ}}$, where eigenfunction intensity is normalized by the its typical value $|\Psi(\mathbf{r})|^2_{\mathrm{typ}}$. The auspicious outcome of this procedure would be vanishing of the size dependence of the far tail statistics. It turns out that, for the same $W = 5$ examples (on 12^3 and 20^3 cubic lattices) shown in Figure 2, $|\Psi(\mathbf{r})|^2_{\mathrm{typ}} V \approx 0.26$ fluctuates only slightly from eigenstate-to-eigenstate or from sample-to-sample. This allows us to define the PT distribution of t',
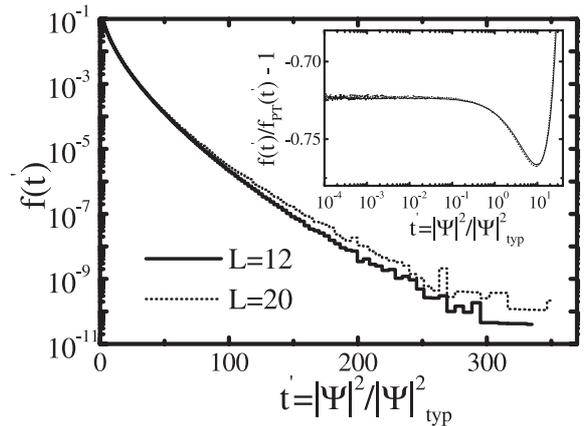

Fig. 9. Distribution function $f(t')$ of the eigenfunction intensities $t' = |\Psi(\mathbf{r})|^2/|\Psi(\mathbf{r})|^2_{\mathrm{typ}}$ (normalized by the typical value of intensity $|\Psi(\mathbf{r})|^2_{\mathrm{typ}}$ of a given eigenstate) in the Anderson modeled nanoscale conductors with $W = 5$ disorder strength on $V = 12^3$ and $V = 20^3$ lattices. This analysis is complementary to that shown in Figure 2 for $f(t)$ where $t = |\Psi(\mathbf{r})|^2/V^{-1}$. The inset plots correction [analogous to the one in Figure 3 for $f(t)$] to the PT distribution $f_{\mathrm{PT}}(t')$ in the region of t' where such deviations are small.

$f_{\mathrm{PT}}(t') = [2\pi t' V|\Psi(\mathbf{r})|^2_{\mathrm{typ}}]^{-1/2} \exp(-t'V|\Psi(\mathbf{r})|^2_{\mathrm{typ}}/2)$. The correction term $f(t')/f_{\mathrm{PT}}(t') - 1$ in the region of small deviations from RMT now displays almost negligible size dependence (see inset in Fig. 9). Nevertheless, Figure 9 shows that size dependence of the far tail of $f(t')$ persists, albeit with a smaller relative difference $|f_{L=12}(t') - f_{L=20}(t')|/f_{L=12}(t')$ than in the case of usual analysis dealing with $f(t)$ in Figure 2.

It remains to be seen if present approaches can combine short-scale effects with those responsible for the size dependence. Namely, ballistic extension of the σ-model [15,42], which attempts to overcome the shortcomings of the diffusion approximation and assumption of slow spatial variation of the NLSM fields, provides a precise numerical coefficient of the log-cube prefactor while leaving its dependence on disorder strength unchanged from $(k_F\ell)^2$ in the diffusive NLSM formalism—this contradicts our findings. On the other hand, DOF technique as formulated in reference [11] is not directly applicable to the conductors modeled by the standard Anderson Hamiltonian [11]. Thus, the structure of eigenfunctions of the Schrödinger equation for a particle in a random potential (which is the basic, tantalizingly simply formulated one-particle quantum-mechanical problem) remains a problem to be elucidated further.

References

1. *Mesoscopic phenomena in solids*, edited by B.L. Altshuler, P.A. Lee, R.A. Webb (North-Holland, Amsterdam, 1991)
2. *Mesoscopic Quantum Physics*, edited by E. Akkermans, J.-L. Pichard, J. Zinn-Justin, Les Houches, Session LXI, 1994 (North-Holland, Amsterdam, 1995)
3. B.L. Al'tshuler, Pis'ma Zh. Eksp. Teor. Fiz. **41**, 530 (1985) [JEPT Lett. **41**, (1985) 648]; P.A. Lee, A.D. Stone, Phys. Rev. Lett. **55**, 1622 (1985)
4. B. Shapiro, Phil. Mag. B **56**, 1031 (1987)
5. P.W. Anderson, Phys. Rev. **109**, 1492 (1958)
6. M. Janssen, Phys. Rep. **295**, 1 (1998)
7. A.D. Mirlin, Phys. Rep. **326**, 259 (2000)
8. Y.V. Fyodorov, A.D. Mirlin, Phys. Rev. B **51**, 13403 (1995)
9. A.D. Mirlin, J. Math. Phys. **38**, 1888 (1997)
10. V.I. Fal'ko, K.B. Efetov, Europhys. Lett. **32**, 627 (1995); V.I. Fal'ko, K.B. Efetov, Phys. Rev. B **52**, 17413 (1995)
11. I.E. Smolyarenko, B.L. Altshuler, Phys. Rev. B **55**, 10451 (1997)
12. V. Uski, B. Mehlig, R.A. Römer, M. Schreiber, Phys. Rev. B **62**, R7699 (2000)
13. B.K. Nikolić, Phys. Rev. B **65**, 012201 (2002)
14. K.B. Efetov, *Supersymmetry in Disorder and Chaos* (Cambridge University Press, Cambridge, 1997)
15. Ya.M. Blanter, A.D. Mirlin, B.A. Muzykantskii, Phys. Rev. B **63**, 235315 (2001)
16. I.E. Smolyarenko, private communication
17. L. Laloux, P. Cizeau, J.-P. Bouchaud, M. Potters, Phys. Rev. Lett **83**, 1467 (1999); V. Plerou, P. Gopikrishnan, B. Rosenow, L.A. Nunes Amaral, H.E. Stanley, Phys. Rev. Lett. **83** 1471 (1999)
18. B.L. Altshuler, V.E. Kravtsov, I.V. Lerner, in reference [1]
19. B.A. Muzykantskii, D.E. Khmelnitskii, Phys. Rev. B **51**, 5480 (1995)
20. C. Basu, C.M. Canali, V.E. Kravtsov, I.V. Yurkevich, Phys. Rev. B **57**, 14 174 (1998)
21. P. Pradhan, S. Sridhar, Phys. Rev. Lett. **85**, 2360 (2000)
22. B.K. Nikolić, P.B. Allen, Phys. Rev. B **63**, R020201 (2001)
23. J.A. Folk *et al.*, Phys. Rev. Lett. **76**, 1699 (1996); A.M. Chang *et al.*, Phys. Rev. Lett. **76**, 1695 (1996)
24. O. Agam, N.S. Wingreen, B.L. Altshuler, D.C. Ralph, M. Tinkham, Phys. Rev. Lett. **78**, 1956 (1997)
25. A.D. Mirlin, Y.V. Fyodorov, J. Phys. A **26**, L551 (1993); Y.V. Fyodorov, A.D. Mirlin, Int. J. Mod. Phys. B **8**, 3795 (1994)
26. Note that in this paper the word "ensemble" denotes our numerically generated set of conductors with different impurity configurations but of the same disorder strength (*i.e.*, impurity concentration). This should not be confused with the word *ensemble* which denotes in random matrix theory a set of all random matrices obeying specific symmetries—the time-reversal and spin-rotation invariant Hamiltonians from each of our "five ensembles" belong to the Gaussian orthogonal *ensemble* of RMT
27. *Chaos in Quantum Physics*, edited by M.-J. Jianonni, A. Voros, J. Zinn-Justin, Les Houches, Session LII, 1989 (North-Holland, Amsterdam, 1991)
28. T. Ghur, A. Müller-Groeling, H.A. Widenmüller, Phys. Rep. **299**, 189 (1998)
29. O. Bohigas, M.J. Giannoni, C. Schmit, Phys. Rev. Lett. **52**, 1 (1984)
30. A.V. Andreev, O. Agam, B.D. Simons, B.L. Altshuler, Phys. Rev. Lett. **76**, 3947 (1996)
31. L.P. Gor'kov, G.M. Eliashberg, Zh. Eksp. Teor. Fiz. **48**, 1407 1965 [Sov. Phys. JETP **21** 1965]
32. B.L. Altshuler, B.I. Shklovskii, Zh. Eksp. Teor. Fiz. **91**, 220 (1986) [Sov. Phys. JETP **64**, 127 (1986)]
33. R.S. Whitney, I.V. Lerner, R.A. Smith, Waves Random Media **9**, 179 (1999)
34. R.E. Prange, Phys. Rev. Lett. **78**, 2280 (1997)
35. A. Altland, C.R. Offer, B.D. Simons, in *Supersymmetry and Trace Formula*, edited by I.V. Lerner, J.P. Keating, D.E. Khmelnitskii, NATO ASI series B, Vol. 370 (Kluwer Publishing, Dodrecht, 1999)
36. Y.V. Fyodorov, in reference [2]
37. C.E. Porter, R.G. Thomas, Phys. Rev. **104**, 483 (1956)
38. F. Haake, *Quantum Signatures of Chaos* (Springer-Verlag, Heidelberg, 2001)
39. L. Kaplan, Phys. Rev. Lett. **80**, 2582 (1998)
40. L.P. Gor'kov, A.I. Larkin, D.E. Khmel'nitskii, Pis'ma Zh. Eksp. Teor. Fiz. **30**, 248 (1979) [JETP Lett. **30**, 228 (1979)]
41. D. Braun, E. Hofstetter, G. Montambaux, A. MacKinnon, Phys. Rev. B **64**, 155107 (2001)
42. B.A. Muzykantskii, D.E. Khmelnitskii, Pisma Zh. Eksp. Teor. Fiz. **62**, 68 (1995) [JETP Lett. **62**, 76 (1995)]
43. V. Uski, B. Mehlig, M. Schreiber, Phys. Rev. B **63**, 241101 (2001)
44. V. Uski, B. Mehlig, R.A. Römer, M. Schreiber, Ann. Phys. (Leipzig) **7**, 437 (1998)
45. G. Montambaux, cond-mat/0012210
46. A.D. Mirlin, Phys. Rev. B **53**, 1186 (1996)
47. B.A. Muzykantskii, D.E. Khmelnitiskii, cond-mat/9601045
48. R. Landauer, Phil. Mag. **21**, 863 (1970); C. Caroli, R. Combescot, P. Nozieres, D. Saint-James, J. Phys. C **4**, 916 (1971)
49. S. Datta, *Electronic Transport in Mesoscopic Systems* (Cambridge University Press, Cambridge, 1995)
50. D. Braun, E. Hofstetter, A. MacKinnon, G. Montambaux, Phys. Rev. B **55**, 7557 (1997)
51. B.K. Nikolić, P.B. Allen, J. Phys. Cond. Matt. **12**, 9629 (2000)
52. Yu.V. Sharvin, Zh. Eksp. Teor. Fiz. **48**, 984 (1965) [Sov. Phys. JETP **21**, 655 (1965)]
53. B.K. Nikolić, Phys. Rev. B **64**, 165303 (2001)
54. N. Argaman, Y. Imry, U. Smilansky, Phys. Rev. B **47**, 4440 (1993)